MULTIPLE DELAYS IN LIGHT CURVES OF LENSED QUASARS

LINDITA HAMOLLI[1], ESMERALDA GULIQANI[2], MIMOZA HAFIZI[1]

[1]Department of Physics, Faculty of Natural Sciences, University of Tirana

[2]Department of Mathematics and Physics, Faculty of Natural and Human Sciences, "Fan S. Noli" University of Korça

e-mail: lindita.hamolli@fshn.edu.al,

Abstract

Measurement of lensed quasar time delays depends on the quality of the light curves obtained in each split image. These delays are created because the light rays of images follow different paths through the gravitational field of the galaxy and can be measured when the source is time-variable. Generally, the source of variability has a finite size, and when it is widely distributed (>100 pc as a whole), variabilities between split images may not show a good correlation. In these cases, multiple different delays can be measured. We investigate this phenomenon in the case of the double lensed quasars that are expected to be observed by the Roman Space Telescope. Using Monte Carlo simulations, we generate quasar-galaxy systems based on the mass-luminosity function of galaxies and the redshift distribution of both galaxies and quasars taken from observations. Relying on the capabilities of the Roman Telescope, we define the lensed quasars, the time delays between images, and time delay differences for the variability source size in the range of 10 to 1000 pc. We find values of time delay differences exceeding 30 days, and these do not depend on the mass distribution of the lens galaxy. We also conclude that in 30% of double lensed quasars, the light curves will not be correlated, and multiple time delays can be measured.

Key words**:** *quasar, galaxy, strong lensing, time delay.*

Përmbledhje

Matja e vonesave kohore të kuazarëve të lensuar varet nga cilësia e kurbave të dritës të marra në çdo imazh të ndarë. Këto vonesa krijohen sepse rrezet e dritës së imazheve ndjekin rrugë të ndryshme në fushën gravitacionale të galaksisë kur burimi është i ndryshueshëm në kohë. Në përgjithësi, burimi i variabilitetit ka një madhësi të kufizuar dhe kur shpërndahet gjerësisht (>100

pc në tërësi), ndryshueshmëritë midis imazheve të ndara mund të mos tregojnë një korrelacion të mirë. Në këto raste, mund të maten vonesa kohore të shumta. Ne e hetojmë këtë fenomen në rastin e kuazarëve të lensuar me dy imazhe që priten të vëzhgohen nga Teleskopi Hapësinor Roman. Duke përdorur simulimet Monte Carlo, ne gjenerojmë sisteme kuazar-galaksi bazuar në funksionin masë-luminositet të galaksive dhe shpërndarjen e redshifteve të galaksive e kuazareve të marra nga vrojtimet. Duke u mbështetur në aftësitë e teleskopit Roman, ne përcaktojmë kuazaret e lensuar, vonesat kohore midis imazheve dhe diferencat e vonesave kohore për madhësinë e burimit të variabilitet në rangun nga 10 deri në 1000 pc. Ne gjejmë vlera të diferencave të vonesës kohore që i kalojnë 30 ditët dhe këto nuk varen nga shpërndarja e masës së galaksisë lente. Gjithashtu, ne konkludojmë se në 30% të kuazareve me dy imazhe, kurbat e dritës nuk do të korrelojnë dhe mund të maten vonesa kohore të shumfishta.

Fjalë kyçe: *kuazar, galaksi, lensimi i fortë, vonesa kohore.*

Introduction

The phenomenon of the gravitationally lensed quasar is used to study galaxy evolution and to constrain cosmological parameters (Refsdal, 1964). This effect occurs when light emitted from a background source (quasar) is deflected due to the gravitational potential of a foreground object, resulting in multiple lensed images of the source. When the quasars are time-variable, the time delays between the lensed images are used to determine the time-delay distance, which is inversely proportional to the Hubble constant, H_0 (Wong et al., 2020). The H_0 value obtained by the distance ladder method with type Ia supernovae and Cepheids is $74.0^{+1.4}_{-1.4}$ km s^{-1}Mpc^{-1} (Riess et al., 2021), which is significantly different from the measurement of $67.4^{+0.5}_{-0.5}$ km s^{-1}Mpc^{-1} obtained by Planck observations of the Cosmic Microwave Background (CMB) (Aghanim et al., 2020). An additional method to determine H_0 is time-delay cosmography.

One of the most successful studies to date has been provided by the H0LiCOW collaboration (Wong et al., 2020), who analysed the time delay of six lensed quasars and found $H_0 = 73.3^{+1.7}_{-1.8}$ km s^{-1}Mpc^{-1}, with an uncertainty of only 2.4%. This result, combined with the other late universe observations (Riess et al., 2021), enhances the H_0 tension up to 5.3σ. However, a more recent analysis of 40 strong gravitational lenses, from TDCOSMO+SLACS (Birrer et al., 2020), has found a value of $67.4^{+4.1}_{-3.2}$ km s^{-1}Mpc^{-1}, relaxing the tension. In this context, further studies including more events are needed for a more

precise estimation of the H_0 parameter. To date, a sample of about 220 lensed quasars are known, however, only a very small subset with multiple well-separated images has been used to measure H_0. In general, in lensed quasars from foreground galaxies, the maximum image separation is ≥1 arcsec (this depends on the angular resolution of the instrument). This is shown in Figure 1, where 90% of the total sample completed it. Monitoring of lensed quasars with image separations smaller than 1 *arcsec* can be provided by future surveys such as the Roman Nancy Grace Space Telescope (Spergel et al., 2015, Hamolli et al., 2023a) and the Vera Rubin Observatory's Legacy Survey of Space and Time (LSST) (Oguri & Marshall, 2010).

Standard time delay calculations assume the source as a point, valid if the size of the source is small compared to the rate of change of the time delay. If the variability inside the source is widely distributed, say over ≥100 pc, the variabilities in the light curves of the lensed images will not show a good correlation and multiple time delays can be measured. QSO 0957+561 provided evidence for multiple delays, with three different time delays found between the two images: 417±0.6 days, 432±1.9 days in the g band, and 425±4 days in the R band (Goicoechea, 2002). Moreover, this event in the radio band gives a time delay with greater uncertainty (Haarsma et al. 1999 found time delays of 409 ± 30 days for this event). Generally, it is accepted that a quasar have an accretion disk (radius, 10^{-2} pc) around a supermassive black hole and a circumnuclear stellar region. It exhibits intrinsic variability due to local phenomena like flares in these regions (range from 10^2 to 10^3 pc). This aligns with Hubble Space Telescope findings on nearby quasars (Bahcall et al.,1997).

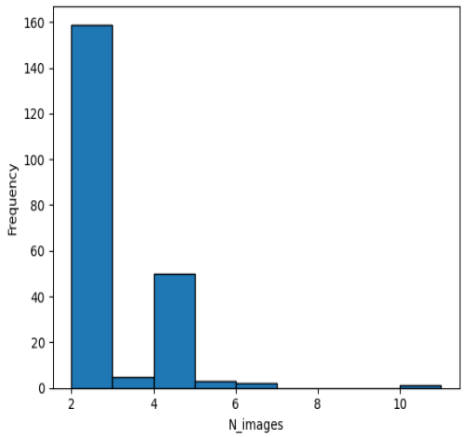

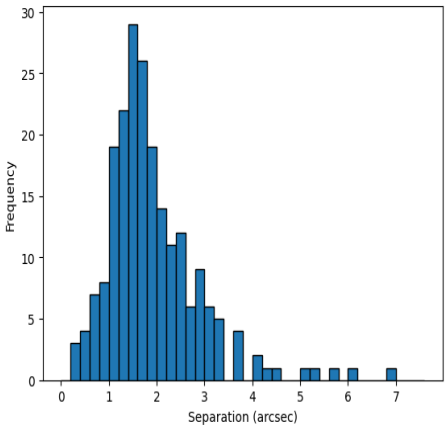

Figure 1. For the 220 known quasars gravitationally lensed by foreground galaxies are shown the number of images and image separation. Left: histogram of known lensed quasars as a function of the number of multiple images (around 160 are double). Right: histogram of known lensed quasars as a function of the maximum image separation. 90% of the lensed quasars have separation between images larger than 1 arcsec. The width of the bin is 0.2 day.

This paper focuses on using the facilities of the Roman Space Telescope to investigate the correlation between those light curves, which are induced by the source of finite size variability. The Roman Space Telescope is a NASA infrared space telescope. It will be positioned at the second Lagrange point (L2) of the Earth-Sun system and will support investigations across nearly all areas of astrophysics, from Solar System studies to cosmology. To achieve this, two instruments will be utilized: the Wide Field Instrument (WFI) and the Coronagraph Instrument. The WFI features eight filter band passes, spanning from 0.48 to 2.3 μm. The Roman survey aims to cover 2,000 square degrees, its angular resolution is 0.1 arcsec[1] and the imaging cadence 5 days (Spergel et al., 2015).

The structure of this paper is organized as follows: Section 2 introduces the fundamental concept of our work and explains the methodology for estimating the time delay difference. In Section 3, we present our algorithm for simulating strong lensing events along with the results derived from it. Finally, Section 4 summarizes the main conclusions drawn from our study.

2. Multiple time delays

When a quasar is lensed by a foreground galaxy, multiple images are formed. Since the most of observed quasars are double, we are focused on this type of them. Let's note its images A and B. If an intrinsic event appears in the light curve of A image, its twin event (a similar feature) is seen in the brightness of B image, and thus, one can measure the corresponding time delay. Following Schneider et al. (1992) when the source centre is placed at an angular position $\vec{\beta}$, two images $\vec{\theta}_A$ and $\vec{\theta}_B$ are defined by the solution of the lens equation:

$$\vec{\beta} = \vec{\theta} - \vec{\alpha}(\vec{\theta}), \quad (1)$$

[1] https://archive.stsci.edu/missions-and-data/roman

where $\vec{\alpha}(\vec{\theta})$ is a bending angle caused by intervening lens object. Standard time delay between images A (at $\vec{\theta}_A$) and B (at $\vec{\theta}_B$) considering the source as a point, is given by

$$\Delta t_{B,A} = \frac{1+z_L}{c}\frac{D_L D_S}{D_{LS}}\left[\frac{1}{2}\left(\vec{\theta}_B - \vec{\beta}\right)^2 - \frac{1}{2}\left(\vec{\theta}_A - \vec{\beta}\right)^2 - \Psi(\vec{\theta}_B) + \Psi(\vec{\theta}_A)\right], \quad (2)$$

where D_L, D_S, D_{LS} are the observer-lens, observer-source, and lens-source angular diameter distances, respectively. z_L is the redshift of the lens, c is the velocity of light in vacuum, and Ψ is the deflection potential, which is directly related to the scaled deflection angle: $\vec{\alpha}(\vec{\theta}) = \vec{\nabla}\Psi(\vec{\theta})$. If the source is aligned with the lens $(\vec{\beta} = 0)$, the Einstein's ring (a critical line) is formed with the angular radius θ_0 given by,

$$\theta_0 = \sqrt{\frac{4GM(\theta)}{c^2}\frac{D_{LS}}{D_L D_S}}, \quad (3)$$

where G is the gravitational constant and $M(\theta)$ is the mass of the lens inside the angle θ. In fact, the quasar has a structure and following the Yonehara´s (1999) explanation, the offset by $\delta\vec{\beta}$ from the source centre will give the offsets $\delta\vec{\theta}_A$ and $\delta\vec{\theta}_B$ of the image positions from their centres, which should fulfil the lens equation again, i.e.,

$$\vec{\beta} + \delta\vec{\beta} = (\vec{\theta}_i + \delta\vec{\theta}_i) - \vec{\alpha}(\vec{\theta}_i + \delta\vec{\theta}_i), \quad i = A \text{ or } B. \quad (4)$$

Subtracting this from equation (1), adopting Taylor expansion to $\vec{\alpha}(\vec{\theta})$ and neglecting the terms higher than first order ($\delta\vec{\beta} \ll \vec{\beta}$, $\delta\vec{\theta}_i \ll \vec{\theta}_i$), one can infer the time delay difference

$$\delta(\Delta t_{B,A}) = \Delta t_{B,A}(\vec{\beta} + \delta\vec{\beta}) - \Delta t_{B,A}(\vec{\beta}) = \frac{1+z_L}{c}\frac{D_L D_S}{D_{LS}}(\vec{\theta}_A - \vec{\theta}_B)\cdot\delta\vec{\beta} \quad (5)$$

Since $\delta\vec{\beta}$ is related with the distance shift in the source plane by $\delta\vec{r} = D_S\delta\vec{\beta}$, Eq. (5) can be rewritten as

$$\delta(\Delta t_{B,A}) = \frac{1+z_L}{c}\frac{D_L}{D_{LS}}(\vec{\theta}_A - \vec{\theta}_B)\cdot\delta\vec{r}\,. \quad (6)$$

It is obvious that the difference in time delay does not depend on the lens model. However, we must emphasize that the positions of the images are dependent on it. This relation is used to define the relative positions of flares that may occur in the structure of quasars (look at Yonehara, 1999;

Goicoechea, 2002 for more details). Below we review two lens galaxy models considered.

- ***Singular Isothermal Sphere (SIS)***

The Singular Isothermal Sphere (SIS) is a simple model that describes the spherical mass distribution with mass density: $\rho = {\sigma_{SIS}}^2/2\pi G r^2$, where σ_{SIS} is the one-dimensional velocity dispersion and r is the distance from the center (Eigenbrod, 2011). Despite its two limitations: the presence of a singularity at the center and an infinite total mass, it does not negate the usefulness of this model to understand the behavior of galactic lenses. For this model one can find the mass inside the angle θ: $M(\theta) = \frac{\pi {\sigma_{SIS}}^2}{G}\theta D_L$ and the angular Einstein radius: $\theta_0 = \frac{4\pi {\sigma_{SIS}}^2}{c^2}\frac{D_{LS}}{D_S}$. When the source lies inside the Einstein ring ($\beta < \theta_0$) the lens equation has two solutions: $\theta_A = \beta + \theta_0$ and $\theta_B = \beta - \theta_0$. The two images are on opposite sides of the lens, with one image (θ_A) inside the Einstein ring and the other (θ_B) outside it. The angular separation between the two images is $\Delta\theta = 2\theta_0$. For the SIS model the standard time delay is calculated by: $\Delta t_{B,A} = \frac{1+z_L}{2c}\frac{D_L D_S}{D_{LS}}(\theta_B^2 - \theta_A^2)$. For this model, the time delay between lensed images are solely due to gravitational effects and the image that is closer to the centre of lens galaxy requires more time to reach the observer (see Hamolli et al., 2023a for more details).

- ***Nonsingular Isothermal Sphere (NIS)***

To smooth out the central singularity in the mass density of the above model we consider Nonsingular Isothermal Sphere (NIS) model with a core region with finite density. Its mass distribution is: $\rho(r) = \frac{{\sigma_{SIS}}^2}{2\pi G}\left(\frac{1}{r^2+r_c^2}\right)$. The core radius r_c is related to the θ_c, by $r_c = \theta_c D_L$. The Einstein angular radius for the NIS model is given by: $\theta_{ENIS} = \theta_0\sqrt{1 - \frac{2\theta_C}{\theta_0}}$, where θ_0 is the Einstein angle for the SIS model. When $\theta_c < \frac{1}{2}\theta_0$, its lens equation has one or three solutions (images) depending on the location of the source. For the NIS model, there is another critical line with angular radius θ_R, which is smaller than the Einstein radius. The corresponding caustic line is a circle with angular radius $\beta_R = \beta(\theta_R)$. For the source located inside the caustic, $\beta < \beta_R$ the lens equation has three real solutions and we consider only the external images (see

Hamolli et al., 2023b for more details). The size of the central core, θ_c affects the positions of the lensed images.

3. Simulations and results

We assume that a strong lensing event is detectable by the telescope if its Einstein angle is higher than the angular resolution of the telescope. To investigate the possibility to observe such events by a telescope, we use the Monte Carlo method to extract all needed parameter. Let's list every step in our algorithm (see Hamolli et al., 2023a for more details):

Based on the quasar distribution determined by Schneider et al. (2005), we calculate the quasar's redshift, then the galaxy's redshift, following their distribution provided by Appenzeller et al. (2004), with the restriction that it is smaller than the quasar's redshift. For each quasar, the total number of galaxies satisfying this condition is determined by the cumulative number of galaxies. For every galaxy generated, we determine its mass using the stellar mass function from Davidzon et al. (2017). Based on the relation between the galaxy's stellar mass and stellar velocity distribution provided by Zahid et al. (2016), we calculate its velocity dispersion. Using the SIS model, we determine the Einstein angle for the quasar/galaxy pair. The probability that a single galaxy resides inside the Einstein angle about the observer–quasar direction is scaled $\theta_0^2/4$. Since Appenzeller et al. (2004) provide the redshift distribution of 7000 galaxies, we normalize the probability considering the whole number of galaxies, 200 billion (0.25 galaxies per arcsec^2, (Beckwith et al., 2006)), and estimate it to be equal to $10^8\,\theta_0^2/14$.

We compare this result with a number n, uniformly distributed in the interval (0, 1), which is extracted by the Monte Carlo code. We keep this pair when its probability is smaller; otherwise, we reject it. The procedure is repeated for all expected quasars to be observed by the Roman Space Telescope. Further, for each aligned quasar/galaxy pair, the positions of images, the time delays $\Delta t_{B,A}$, between them, and the time delay difference, $\delta(\Delta t_{B,A})$ when a $\delta\vec{r}$ randomly distribution in range [10, 1000] pc, are calculated. Moreover, for the aligned quasar-galaxy pair, we also consider the NIS model doing the same calculations as in the SIS. Since we require three real images for the quasar/galaxy pair, we generate a random $\theta_c < \left(\frac{1}{2}\right)\theta_0$ until it fulfils the condition $\beta < \beta_R$ (Hamolli et al., 2023b).

For our calculations we have assumed the a flat Universe and three angular diameter distances are found by: $D_L = \frac{c}{H_0(1+z_L)} \int_0^{z_L} \frac{dz}{E(z)}$, $D_S = \frac{c}{H_0(1+z_S)}$; $D_{LS} = D_S - \frac{1+z_L}{1+z_S} D_L$; $E(z) = \sqrt{\Omega_m(1+z)^3 + \Omega_k(1+z)^2 + \Omega_\lambda}$. Here, Ω_m, Ω_k, Ω_λ are the dimensionless density parameters, i.e. the sum of the cold dark matter and the baryonic matter, the space-curvature, and the dark energy, respectively. The values used for these parameters are as follows: $\Omega_m = 0.30, \Omega_k = 0, \Omega_\lambda = 0.70$ and $H_0 = 70$km s^{-1} Mpc^{-1} (Liao, 2019).

Based on the algorithm described above, we generate a sample of 100,000 strong lensing events. By comparing the Einstein angle of the pair with the angular precision of the Roman telescope, which is 0.1 arcsec, we find lensed quasars. Around 85% of these are lensed by a single galaxy, resulting in a double quasar. The number of events from our sample that meet the above conditions is 527.

For these, we calculate the position of the two images, time delays $\Delta t_{B,A}$, and then time delay difference, $\delta(\Delta t_{B,A})$, considering a source size of the variability randomly distributed in range [10, 1000] pc.

Figure 2 shows the scatter of the values of $\delta(\Delta t_{B,A})$ for the two considered models, SIS and NIS. As can be observed, their values range from 0 to over 30 days and do not depend on the galaxy model (the slope is 0.96). If we formulate equation (6) for the two models and then calculate the ratio between the time delay differences, it turns out to be equal to the ratio of their angular

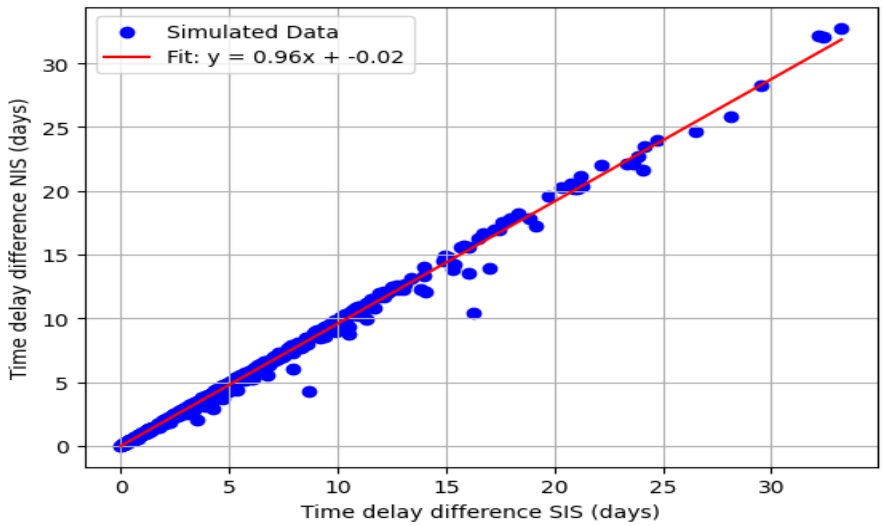

separations between lensed images. The differences between the angular separations for the two models are very small, hence the scatter is nearly linear.

Figure 2. This figure presents a scatter plot of the time delay differences between the lensed images of double quasars, expected to be observed by the Roman Telescope. The analysis considers two models, SIS and NIS. The curve of best fit is represented by the red line.

Figure 3 presents the scatter of the time delay difference by the radius of the source variability for the two models under consideration. Variable source radius values are randomly simulated within the interval of [10, 1000] pc. As can be seen, there is a tendency: as the radius of variability increases, so does the time delay difference. To verify this, we calculate the statistical coefficients of Pearson and Spearman. Pearson's correlation of 0.55 suggests a positive linear relationship, while Spearman's correlation of 0.68 indicates a monotonic increase, but not at a constant rate. These trends are consistent across both models.

Figure 4 depicts the histogram of the time delay differences for 527 double quasars. The radius of the source variability ranges from 10 to 1000 pc. The SIS model is represented by the grey shaded area, and the NIS model is represented by the red line. Each bin has a width of 1 day, and the average time delay difference is 6.2 days. As observed, most of the events have a time delay difference of less than 5 days. Since the Roman Telescope is scheduled to capture images every 5 days, we can infer that in most instances, there will be a correlation between the light curves of the lensed images. Taking into consideration only the time delay differencies higher than 5 days, we find a number of 160 events, which are 30% of the total number of events.

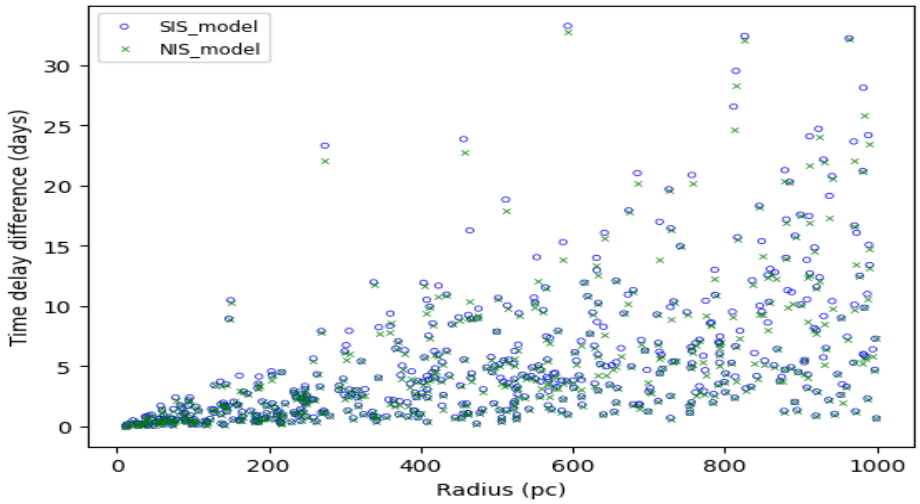

Figure 3. This figure shows the scatter plot of the relationship between the time delay differences of lensed images and the radius of the source variability. The radius values span from 10 pc to 1000 pc.

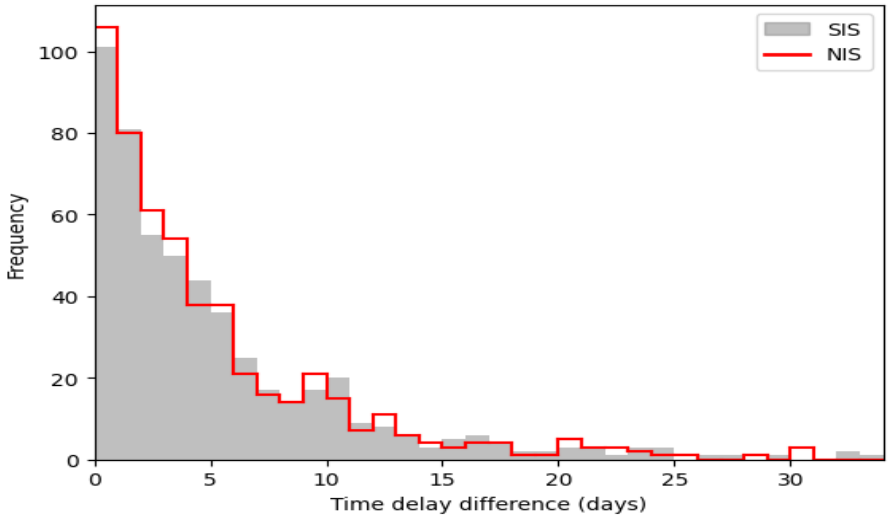

Figure 4. This figure illustrates the frequency of time delay differences between two lensed images for both the SIS (the grey shaded area) and NIS (the red line) models. The sample contains 527 events. The width of each bin is 1 day.

Conclusions

In this paper, we have investigated the impact of the size of the source variability on the light curves of lensed images expected to be observed by the Roman Telescope. By comparing the phases of the light curves, when they are not correlated with each other, the multiple time delays can be measured. One of the contributing factors to this phenomenon is the finite size of the variability source, which increases the uncertainty in defining the time delay and consequently to constrain the Hubble constant.

Since most of the lensed quasars observed are double, we have considered the quasars lensed by a galaxy. We find that 85% of the lensed quasars expected to be observed by the Roman Telescope are double.

Even if the measurement of the time delay between lensed images provides a good method, it is influenced by the uncertainties inherent in the time delay measurements. The periodic observations (imaging cadence) are very important for the accuracy of the time delay measurement. Considering the variability radius of the quasar in the range [10, 1000] pc, we find that the values of the time delay difference, $\delta(\Delta t_{B,A})$, vary from 0 days to over 30 days. Since the imaging cadence of the Roman Telescope is 5 days, a correlation between the light curves is expected in most of the lensed quasars that it observes. However, our findings suggest that only in 30% of these quasars will show a non-correlation, allowing for the measurement of multiple time delays.

Since non-correlated light curves can also form when flares occur in the quasar's accretion disks or circumnuclear stellar regions, researchers can analyse them to determine the relative positions of the two lensed images. For more details, refer to the work by Goicoechea in 2002. Understanding these non-correlated features is crucial for unravelling the quasar's structure.

References

Aghanim, N., Akrami, Y., Ashdown, M., Aumont, J., Baccigalupi, C., Ballardini, M., Banday, A. J., Barreiro, R. B., Bartolo, N., Basak, S., Battye, R. A., Benabed, K., Bernard, J., Bersanelli, M., Bielewicz, P., Bock, J. J., Bond, J. R., Borrill, J., Bouchet, F. R., Zonca, A. (2020). *Planck* 2018 results. *Astronomy and Astrophysics*, *641*, A6. https://doi.org/10.1051/0004-6361/201833910

Appenzeller, I., Bender, R., Böhm, A., Stephan, F., Fricke, K. J., Gabasch, A., Heidt, J., Hopp, U., Jäger, K., Mehlert, D., Noll, S., Saglia, R., Seitz, S., Tapken, C., & Ziegler, B. (2004). Exploring Cosmic Evolution with the FORS Deep Field. The Messenger, 116, 18–24. http://pubman.mpdl.mpg.de/pubman/item/escidoc: 949258

Bahcall, J.N., Kirhakos, S., Saxe, D.H. and Schneider, D.P., (1997). Hubble space telescope images of a sample of 20 nearby luminous quasars. The Astrophysical Journal, 479(2), p.642.

https://doi.org10.1086/303926/

Beckwith, S., Stiavelli, M., Koekemoer, A. M., Caldwell, J. a. R., Ferguson, H. C., Hook, R. N., Lucas, R. A., Bergeron, L., Corbin, M. R., Jogee, S., Panagia, N., Robberto, M., Royle, P., Somerville, R. S., & Sosey, M. (2006). The Hubble Ultra Deep field. The Astronomical Journal, 132(5), 1729–1755. https://doi.org/10.1086/507302

Birrer, S., Shajib, A.J., Galan, A., Millon, M., Treu, T., Agnello, A., Auger, M., Chen, G.F., Christensen, L., Collett, T. and Courbin, F. (2020). TDCOSMO-IV. Hierarchical time-delay cosmography–joint inference of the Hubble constant and galaxy density profiles. Astronomy & Astrophysics, 643, p.A165. https://doi.org/10.1051/0004-6361/202038861

Davidzon, I., Ilbert, O., Laigle, C., Coupon, J., McCracken, H. J., Delvecchio, I., Masters, D., Capak, P., Hsieh, B. C., Le Fèvre, O., Tresse, L., Bethermin, M., Chang, Y. -Y., Faisst, A. L., Le Floc'h, E., Steinhardt, C., Toft, S., Aussel, H., Dubois, C., Hasinger, G., Salvato, M., Sanders, D. B., Scoville, N., Silverman, J. D. (2017). The COSMOS2015 galaxy stellar mass function. Thirteen billion years of stellar mass assembly in ten snapshots. Astron. Astrophys, 605, A70. https://doi.org/10.1051/0004-6361/201730419

Eigenbrod. A., (2011). Gravitational lensing of quasars. CRC Pres.

Goicoechea, L.J., (2002). Multiple delays in QSO 0957+ 561: observational evidence and interpretation. Monthly Notices of the Royal Astronomical Society, 334(4), pp.905-911. https://doi.org/10.1046/j.1365-8711.2002.05574.x

Haarsma, D.B., Hewitt, J.N., Lehar, J. and Burke, B.F. (1999). The radio wavelength time delay of gravitational lens 0957+ 561. The Astrophysical Journal, 510(1), p.64. https://doi.org/10.1086/306584

Hamolli, L., Hafizi, M., De Paolis, F., Guliqani, E., (2023a). Investigating Gravitationally Lensed Quasars Observable by Nancy Grace Roman Telescope. Galaxies 2023, 1, 0. https://doi.org/10.3390/galaxies11030071

Hamolli, L., Guliqani, E., Hafizi, M. (2023b). THE INFLUENCE OF THE LENS MODEL ON TIME DELAY DURING STRONG LENSING BY GALAXIES. Journal Natyral Science, No.33, p. 3-20. Publication no.33, year 2023 – JNS

Liao, K., (2019). Measuring the Distances to Quasars at High Redshifts with Strong Lensing. The Astrophysical Journal, 883(1), 3. https://doi.org/10.3847/1538-4357/ab39e6

Oguri, M. and Marshall, P.J. (2010). Gravitationally lensed quasars and supernovae in future wide-field optical imaging surveys. Monthly Notices of the Royal Astronomical Society, 405(4), pp.2579-2593. https://doi.org/10.1111/j.1365-2966.2010.16639.x

Refsdal, S. (1964). On the Possibility of Determining Hubble's Parameter and the Masses of Galaxies from the Gravitational Lens Effect. Monthly Notices of the Royal Astronomical Society, 128(4), 307–310. https://doi.org/10.1093/mnras/128.4.307

Riess, A. G., Casertano, S., Yuan, W., Bowers, J. B., Macri, L. M., Zinn, J., & Scolnic, D. (2021). Cosmic Distances Calibrated to 1% Precision with Gaia EDR3 Parallaxes and Hubble

Space Telescope Photometry of 75 Milky Way Cepheids Confirm Tension with ΛCDM. The Astrophysical Journal, 908(1), L6. https://doi.org/10.3847/2041-8213/abdbaf

Schneider, D. P., Hall, P. B., Richards, G. T., Vanden Berk, D. E., Anderson, S. F., Fan, X., Jester, S., Stoughton, C., Strauss, M. A., SubbaRao, M., Brandt, W. N., Gunn, J. E., Yanny, B., Bahcall, N. A., Barentine, J. C., Blanton, M. R., Boroski, W. N., Brewington, H., Brinkmann, J.,York, D. G. (2005). The Sloan Digital Sky Survey Quasar Catalog. III. Third Data release. The Astronomical Journal, 130(2), 367–380. https://doi.org/10.1086/431156

Schneider, P., Ehlers, J., & Falco, E. (1992). Gravitational lenses. In Astronomy and astrophysics library. https://doi.org/10.1007/978-3-662-03758-4

Spergel, D. N., Gehrels, N., Baltay, C., Bennett, D. P., Breckinridge, J. B., Donahue, M., Dressler, A., Gaudi, B. S., Greene, T. P., Guyon, O., Hirata, C., Kalirai, J., Kasdin, N. J., Macintosh, B., Moos, W., Perlmutter, S., Postman, M., Rauscher, B. J., Rhodes, J., . . . Zhao, F. (2015). Wide-Field InfraRed Survey Telescope-Astrophysics Focused Telescope Assets WFIRST-AFTA 2015 Report. arXiv (Cornell University). http://arxiv.org/pdf/1305.5422.pdf

Yonehara, A., (1999). Source size limitation from variabilities of a lensed quasar. The Astrophysical Journal, 519(1), p. L31. https://doi.org/10.1086/312107

Zahid, H. J., Geller, M. J., Fabricant, D. G., & Hwang, H. S. (2016). The scaling of stellar mass and central stellar velocity dispersion for quiescent galaxies at z< 0.7. The Astrophysical Journal, 832(2), 203. https://doi.org/10.3847/0004-637x/832/2/203

Wong, K., Suyu, S., Chen, G., Rusu, C., Millon, M., Sluse, D., Bonvin, V., Fassnacht, C., Taubenberger, S., Auger, M., et al. (2020). H0LiCOW–XIII. A 2.4 per cent measurement of H0 from lensed quasars: 5.3 σ tension between early-and late-Universe probes. Mon. Not. R. Astron. Soc. 2020, 498, 1420–1439. https://doi.org/10.1093/mnras/stz3094